JOURNAL OF MATERIALS SCIENCE 32 (1997) 5577–5581

# Electrical resistance as a tool in determining the failure of fibres in a nicalon-reinforced LAS glass-ceramic with $Ta_2O_5$ additions

G. R. VILLALOBOS, R. F. SPEYER
*School of Materials Science and Engineering, Georgia Institute of Technology, Atlanta, GA 30332, USA*

The electrical resistance of a Nicalon-reinforced lithium aluminosilicate glass-ceramic with $Ta_2O_5$ additions was used as an indicator of fibre and TaC/Carbon coating fracture during flexural testing. The resistivities of fibres in the composite were significantly lower than the free fibres owing to the high conductivity carbon and TaC coatings which formed during hot pressing. Hot-pressing times beyond 0.5 h resulted in a degradation of flexural strength via the formation of a strongly bonded TaC layer at the expense of the carbon debond layer.

## 1. Introduction

A drawback of using ceramic materials in structural applications is the uncertainty associated with the nature and distribution of imperfections which, in turn, dictates fracture strength. In a fibre-reinforced ceramic composite, if the fibres are electrically conductive, fibre fracture would be manifested as an increase in resistance in the fibre direction. Thus, measurement of the resistance of a part in service might be used to detect impending mechanical failure.

Using the resistance of a composite as a means of determining crack length during fatigue testing has been attempted in the past on fibre-reinforced polymer matrix materials with mixed success. Prabhakaran [1] treated the fibres as parallel resistors with a series resistance comprising electrical contacts and lead wires. The change in resistance was calculated as a function of the depth of cut into the cross-section of a carbon fibre-reinforced polymer composite, based on free fibre resistance. The author indicated that the uncertainty of the contact resistances in series with the fibres could be used to explain differences between calibration curves derived from actual incisions into a composite cross-section, and calculations based on free fibre resistance. Muto and Yanagida [2] explored the feasibility of using electrical resistance to predict the fracture of a carbon/fibre-reinforced plastic composite. They were able to measure an increasing resistance associated with the fracture of individual fibres, but were unable to predict the on-coming maximum load in time to stop catastrophic failure.

Ceramic composite failure models [3–6] suggest that failure of a ceramic composite consists of matrix micro-cracking, matrix crack propagation, fibre–matrix debonding, fibre failure, and pullout of the reinforcing fibres. Not all of these steps are manifested in all composites, and may not be sequential. It has been generally assumed that for composites with graceful (e.g. tough) failure characteristics, a very low percentage of the fibres fractured prior to total matrix failure. The degradation in strength after the peak load (ultimate strength) would be due to progressive individual fibre failure and frictional resistance via fibre pullout.

Prewo *et al.* [7] found Nicalon fibre (composed of ultrafine β-SiC crystals with excess carbon and 9%–11% oxygen as $SiO_2$ [8])-reinforced lithia aluminosilicate (LAS) composites displayed graceful failure due to a carbon debond layer that formed between the fibres and the LAS matrix. The carbon layers formed [9–12] via $SiC + O_2 = SiO_2 + C$ or $SiC + 2CO = SiO_2 + 3C$. Exposure of the composite to temperatures above 800 °C in air resulted in degradation of the carbon coating and a severe decrease in strength. Additions of $Ta_2O_5$ to the LAS matrix has been shown to increase the elastic modulus and ultimate strength of the composite [13]. TaC coatings form around the Nicalon fibres via reaction between carbon coatings and $Ta_2O_5$ ($Ta_2O_5 + 7C = 2TaC + 5CO$). As shown in previous work [14], increased hot-pressing periods facilitated greater formation of TaC, as $Ta_2O_5$ in the fluid matrix could, with time, migrate to near-fibre regions where it would react.

## 2. Experimental procedure

Lithium carbonate (J. T. Baker, 99.2% pure), alumina (Alcoa A15 SG) and silica (Johnson Matthey, 99.5% pure) were mixed to form an overall composition of $1Li_2O$–$1Al_2O_3$–$4SiO_2$. $Ta_2O_5$ (Johnson Matthey, 99.9% pure) powders were added to the LAS batch in the amounts of 6%, 9% and 15% of the total moles of LAS. Compositions will henceforth be designated, for example, as 6% $Ta_2O_5$, to represent the LAS glass with 6% $Ta_2O_5$ additions. Powder mixtures

0022–2461  

were placed in alumina crucibles, and melted via a $MoSi_2$-element furnace in air, heating at 10 °C min$^{-1}$ to 1600 °C, and held at that temperature for 4 h. The melts were then quenched on to a chrome-coated steel plate. The resulting glasses were crushed using an alumina mortar and pestle to $-230$ mesh (63 μm opening), and shown to be amorphous using X-ray diffraction.

The Nicalon-reinforced glass-ceramic composites were fabricated using a slurry infiltration technique [14]. The glass powders were suspended in a mixture of 2% (by weight) polyvinyl alcohol and 98% water. The fibre tows were placed in a grafoil box and the solution was poured over the fibres. The infiltrated fibres were dried in air at 100 °C for 3 h, and heated at 10 °C min$^{-1}$ to 600 °C to burn out the PVA binder.

Hot pressing was performed using an induction heated graphite die. The inner portion of the die and the ends of the punches were lined with Grafoil. The die was surrounded with alumina bubble insulation and was contained in a silica sleeve. Argon flowed into the assembly through the bottom of the silica sleeve and was exhausted at the top. Pressure was applied through a hydraulic ram and temperature was measured with a thermocouple junction embedded in the die wall. Ram travel (sample densification) was measured with a dial gauge, accurate to 0.01 mm. A typical temperature/heating schedule consisted of heating to 1400 °C at 70 °C min$^{-1}$ and 0.5 MPa, soaking for 30 min to 2 h at 5 MPa, and then turning the power off to cool. Test bars of dimensions of approximately $2.0 \times 1.5 \times 40$ mm$^3$, roughly corresponding to ASTM C 1161–94 size *A*, were cut from the hot-pressed shape with a diamond wafering blade and were ground with 600 grit silicon carbide paper.

Electrical connections were made to the test bars by coating the ends with silver paste and affixing silver wire. Resistance was measured using a Keithley 196 DMM with a resolution of 100 μΩ. During mechanical testing, the resistance was continuously monitored and stored on a computer at 1 s intervals. Flexural tests were made in three-point bending mode (ASTM C 1161–94 size *A*) with a bottom span of 20 mm, pins of 2–2.5 mm diameter, and a crosshead speed of 0.2 mm min$^{-1}$. The screw drive load frame was controlled, and the test data were collected by a microprocessor-based (Phoenix Measurement Technology Inc., Roswell GA) system. Average properties and standard deviations were calculated based on stress–strain curves from four or five specimens cut from the identical hot-pressed specimen. Toughness was calculated by integrating the area under each stress–crosshead displacement curve. The upper integration limit was specified at a crosshead displacement of 1 mm (300 s). A pseudo-yield strength was calculated based on a 0.2% strain offset from elastic extension. The interfacial shear strengths of the composites were measured using the technique developed by Marshall [15]. The samples were mounted in epoxy with the fibre axes perpendicular to the polished surface. A Leico microhardness tester (cited above) using a Vickers indentor and 100 g load was used to perform the measurements [14].

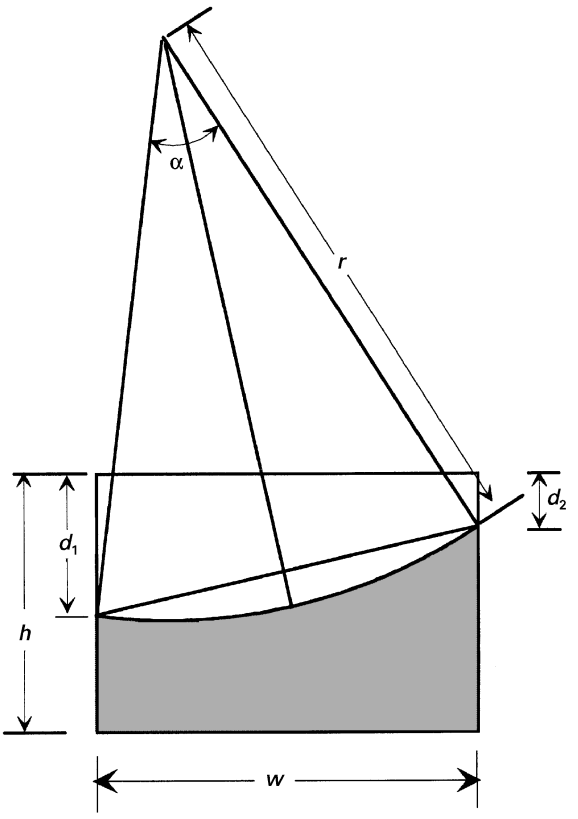


*Figure 1* Method for calculating the area due to the curvature of the wafering blade. Specimen cross-section and blade radius are not to scale.

The resistance of free fibres was measured across a 40 mm length of a desized tow which consisted of 500 individual fibres. The fibres were spread out and affixed to a glass slide using carbon tape, where the upper surface of the tape was coated with silver paste. Silver wires were imbedded in the silver paste at each end, from which the resistance of the fibre tow was measured. The resistance of the individual fibres was calculated based on this resistance multiplied by the number of parallel fibres. The resistance of the matrix alone was measured using a 20 mm diameter × 3 mm thick LAS 6%$Ta_2O_5$ hot-pressed disc, using silver paste and wires, as before.

To correlate the number of fibres broken to the measured resistance, deeper incisions into the cross-sectional areas of four test bars were progressively made via diamond-tipped wafering blade (cutting perpendicular to the fibre direction). The depths of the cuts along the two specimen side walls were measured using an optical microscope with a measuring device accurate to 1 μm (Leico M 400F, St Joseph, MI). The additional area cut due to the curvature of the diamond wafering blade was calculated by subtracting the area of the triangle (of angle α and side *r*) from the area of the wedge (Fig. 1). Thus, the fraction area removed from the cross-section is

$$f = r\left[ r\sin^{-1}\left\{\frac{[(d_1 - d_2)^2 + w^2]^{1/2}}{2r}\right\}\right.$$

$$\left. - [(d_1 - d_2)^2 + w^2]^{1/2}\right.$$

$$\times \cos\left(\sin^{-1}\left\{\frac{[(d_1 - d_2)^2 + w^2]^{1/2}}{2r}\right\}\right)\Bigg] + d_2 w + \frac{(d_1 - d_2)}{2}\Bigg/(hw) \quad (1)$$

where $w$ and $h$ were the individually measured widths and heights of individual cross-sections, respectively, and $d_1 \leqslant d_2$. The radius of the blade, $r$, was 50.8 mm. The fraction of severed fibres was assumed to be equal to the fraction of the cross-sectional area removed. The results were plotted as the change in resistance per unit original (un-cut) resistance versus the fraction severed.

## 3. Results

The resistance of the matrix consolidated with no fibres was beyond the measuring capabilities of the multimeter (300 MΩ). The reinforcing Nicalon fibres were thus taken to be parallel resistors of equal resistance embedded in a matrix with infinite resistance. Thus, the composite resistance was the average resistance of an individual fibre divided by the total number of fibres in the bar. It was assumed that the 125 000 fibres (250 tows) were uniformly distributed throughout the hot-pressed shape. Based on resistance measurements of desized Nicalon fibres, fibre resistivity was calculated to be 7000 Ωcm, which is within the 1000–10 000 Ωcm range specified by the manufacturer [8]. However, calculations based on resistance measurements of the test bars show a fibre resistivity of 0.004 Ωcm.

Fig. 2 shows the calculated change in relative resistance with decreasing number of intact fibres, based on the assumption of uniformly distributed fibres, and

$$\frac{\Delta R}{R_0} = \frac{f}{1 - f} \quad (2)$$

The data markers in the figure represent a variety of $Ta_2O_5$ concentrations and hot-pressing soak periods. The data appeared to follow the same trend regardless of composition/thermal schedule. A sixth-order polynomial was fit to these data, and is overlayed in the figure.

Table I lists the average value and standard deviations of yield strength, ultimate strength, toughness and interfacial shear strength. The average ultimate strength of the composite decreased from 374 MPa to 113 MPa with increasing hot-pressing time from 30 min to 1 h. Thereafter, intermediate average ultimate strengths were measured, but with a significantly greater spread in the data. Similar effects are apparent in measured yield strengths and toughnesses. The hot-pressing schedule with a 1 h soak time was repeated to confirm the drop in strength/toughness. For the same soak period (0.5 h), there was no statistically significant change in mechanical properties with increasing $Ta_2O_5$ content. The average interfacial shear strengths of the 6%$Ta_2O_5$ samples hot pressed for 0.5, 1 and 1.5 h were statistically the same. Only the interfacial shear strength of the 2 h sample was higher. Increasing $Ta_2O_5$ concentrations did not result in statistically significant increases in interfacial shear strength.

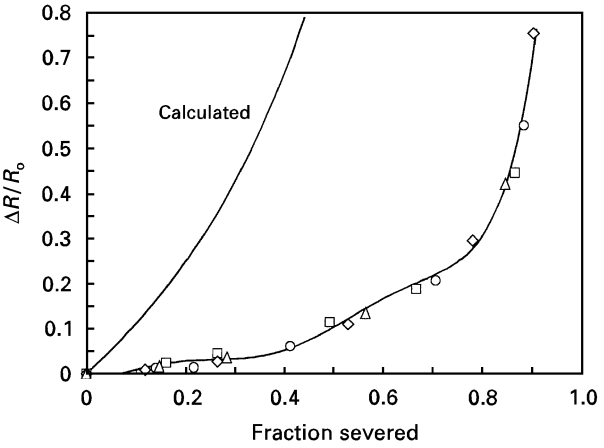


*Figure 2* Resistance behaviour as a function of cross-sectional area removed. Data markers show measured relative resistances of partially cut cross-sections, for specimens hot pressed at 1400 °C and 5 MPa. (○) 6%$Ta_2O_5$ hot pressed for 0.5 h, (□) 6%$Ta_2O_5$ hot pressed for 2 h, (◇) 9%$Ta_2O_5$ hot pressed for 0.5 h, (△) 15%$Ta_2O_5$ hot pressed for 0.5 h. The curve going through the data markers represents a sixth-order best-fit polynomial.

Fig. 3a–e show various samples after fracture under flexural loading. For the 6%$Ta_2O_5$ sample hot pressed for 0.5 h, the compressive side (top) of the test bar shows compressive failure to a point well below the original neutral axis (centreline). Tensile failure is only apparent in the lower third of the test bar. Both

TABLE I Mechanical properties of composites ± 1 S.D.

| Sample | Ultimate strength (MPa) | Yield strength (MPa) | Toughness (J mm$^{-2}$) | Interfacial shear strength (MPa) |
|---|---|---|---|---|
| 6%$Ta_2O_5$ | | | | |
| 0.5 h | 374 ± 13 | 298 ± 28 | 303 ± 42 | 17 ± 6 |
| 1.0 h | 113 ± 17 | 80 ± 27 | 50 ± 25 | 20 ± 2 |
| 1.0 h | 122 ± 40 | 77 ± 9 | 49 ± 10 | 21 ± 8 |
| 1.5 h | 229 ± 112 | 198 ± 101 | 163 ± 93 | 19 ± 11 |
| 2.0 h | 156 ± 101 | 144 ± 98 | 96 ± 63 | 50 ± 23 |
| 9%$Ta_2O_5$ | | | | |
| 0.5 h | 286 ± 63 | 222 ± 39 | 145 ± 94 | 26 ± 13 |
| 15%$Ta_2O_5$ | | | | |
| 0.5 h | 381 ± 60 | 354 ± 83 | 241 ± 123 | 27 ± 16 |

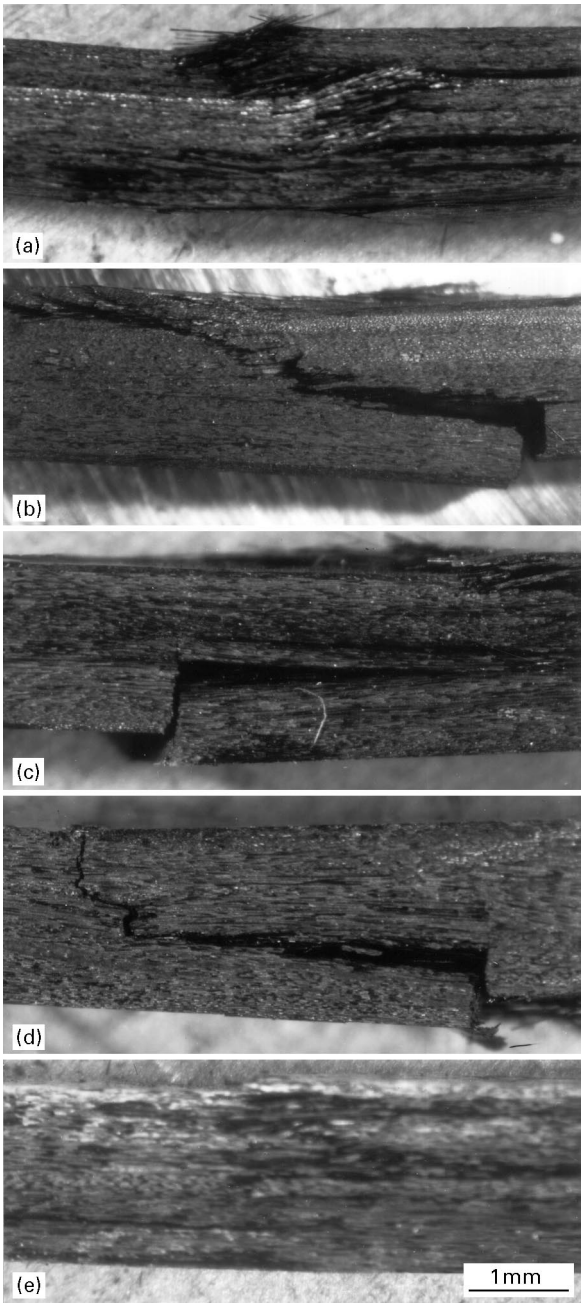


*Figure 3* Optical micrograph of 6%$Ta_2O_5$ samples hot pressed for (a) 0.5 h, (b) 1 h, (c) 1.5 h, and (d) 2 h. (e) Optical micrograph of 15%$Ta_2O_5$ sample hot pressed for 0.5 h. All five samples were hot pressed at 1400 °C and 5 MPa. In all figures, loading was applied so as to put the lower surface in tension.

the compressive and tensile portions of the bar show extensive fibre debonding from the matrix. At the other extreme, the 6%$Ta_2O_5$ sample hot pressed for 2 h shows no evidence of compressive failure; the crack progressed perpendicular to the fibre direction until extended delamination shifted the axial position of the crack. The entirety of the fracture appears to be the result of a tensile failure. The 1 and 1.5 h samples show intermediate amounts of compressive failure, but along with the 2 h sample, show minimal individual fibre debonding. The sample containing 15% $Ta_2O_5$ hot pressed for 0.5 h (Fig. 3c) shows less compressive failure, with fibre debonding similar to the sample with 6%$Ta_2O_5$ hot pressed for 0.5 h.

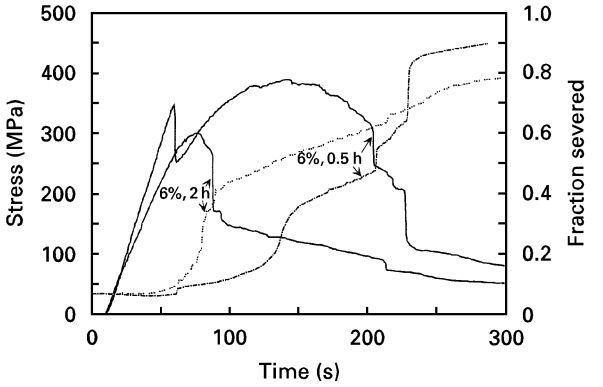


*Figure 4* Stress and fraction served as a function of time under a loading rate of 0.2 mm $min^{-1}$ for samples hot pressed at 1400 °C at 5 MPa for the 6%$Ta_2O_5$ composition for the indicated hot pressing times. The discontinuous lines are fraction severed and the solid lines are stress.

Fig. 4 shows the superimposed stress–time and fraction severed curves for 6%$Ta_2O_5$ samples hot pressed for 0.5 and 2 h. Fraction severed results were determined from relative resistance measurements converted using the polynomial function plotted in Fig. 2. The stress–time curve for the 6%$Ta_2O_5$–0.5 h sample shows a considerable toughness, while the 6%$Ta_2O_5$–2 h sample was less so. As long as the early stress/time slope was constant, no fibre fracture is indicated. However, decreases in slope as the first maximum in strength is approached, coincide with increases in fraction severed. The fraction severed curves for the 6%$Ta_2O_5$ samples show distinct increases in slope after ultimate strengths were reached; later discontinuous increases in fraction severed coincide with significant drops in strength.

## 4. Discussion

As the hot-pressing period was increased past 0.5 h, the extent of fibre debonding (Fig. 3) was diminished. This can be attributed to TaC formation to the point that the continuity of the carbon debonding layer was lost, and direct bonding between the fibre and TaC resulted. Fracture behaviour did not appear to differ with increasing $Ta_2O_5$ concentrations; compressive failure was apparent on the top surface, and appreciable debonding can be seen through the composite interior: the availability of $Ta_2O_5$ with an additive concentration of 6% and above was adequately high whereby concentration was not a factor, and degradation of the carbon layer in favour of TaC was dependent only on the time of heat treatment.

A clearly higher yield and ultimate strength was measured for the 6%$Ta_2O_5$ specimen hot pressed for 0.5 h than for longer hot-pressing periods; appreciable debonding in the fracture behaviour shown in Fig. 3 facilitated the higher measured strengths. Variability in ultimate strengths was much greater for the longer hot-pressing times of 1.5 and 2 h. In these cases, the composites were behaving more as monolithic ceramics, where the stress at fracture would be dependent on the flaw distribution within it, which would vary from specimen to specimen. Interfacial shear strength

measurements showed a distinct increase after a longer soak period (2 h) than the measured decrease in strength (1 h). However, photomicrographs clearly show enhanced debonding in composites with higher ultimate strengths.

The reduction in resistivity of fibres in the hot-presssed composite as compared to free fibres is interpreted to be related to the concentric carbon and TaC coatings ($\rho_{graphite} = 65\ \mu\Omega cm$, $\rho_{TaC} = 30\ \mu\Omega cm$) which formed around the Nicalon fibres. Calculations placing the fibre, carbon coating, and TaC coating as parallel resistors show that as little as a 0.05 μm continuous carbon coating, or a 0.25 μm TaC coating, could have lowered the resistivity of the coated fibre to the 0.004 Ωcm measured in the hot-pressed test bars.

Coating formation during hot-pressing did not change the values of $\Delta R/R_0$ (see resistance independence in Equation 2). Thus, this phenomenon cannot be used to explain the difference between calculated (based on free-fibre) and composite-measured resistances shown in Fig. 2. This difference can be explained based on an increase in series resistance [1] for the composite measurements. In the ratio $\Delta R/R_0$, only the denominator is increased with increasing series resistance, whereby the ratio is decreased for a given fraction severed.

The relative resistances shown in Fig. 2 do not show scatter based on hot-pressing period or composition. This is a result of using relative resistance as the ordinate which is normalized for the original (unsevered) values of resistance. The fraction severed values in Fig. 4 do not start at values of zero because the polynomial fit (Fig. 2) does not deviate from the baseline until a fraction severed of 0.1.

The effect of substantially lowered resistivity due to the fibre coatings suggests the possibility that some of the increased fraction severed indicated during mechanical testing may be due to fracture of the coating without actual fibre breakage. For the 6%$Ta_2O_5$ composition hot pressed for 2 h, fibre fracture, as opposed to fibre debonding, was shown to be the dominant mechanism of composite failure. Thus, in this case, the distinct increase in fraction severed slope leading up to the ultimate strength can be attributed strictly to simultaneous fracture of fibres and coatings. However, for the 6%$Ta_2O_5$ compositions hot pressed for 0.5 h, the increase in indicated fraction severed leading up to the ultimate strength is likely to be a result of fibre matrix debonding. The fibres will tend to debond at the TaC–carbon interface [14], damaging the continuity of both carbon and TaC layers, increasing the measured resistance. In the process of fibre debonding, multiple matrix cracking occurs to the point where the entirety of the load is taken over by the still-intact fibres. Thus, the small increases in fraction severed associated with this phenomenon would not be indicative of fibre fracture. However, the fraction severed trace does clearly indicate changes in the composite which closely parallel features in the stress–strain behaviour. Past the ultimate strengths, the sharp increases in fraction severed are clearly due to fracture of fibres (and their coatings).

## 5. Conclusion

The ultimate strengths of the composites were sensitive to the time permitted for TaC formation, but not the availability (concentration) of $Ta_2O_5$. Measured resistances of the composite were calibrated to indicate the fraction of fibres, or their C/TaC coatings, severed. Fraction severed plots showed sensitivity to both fibre debonding and fracture.

## References


1. R. PRABHAKARAN, *Exp. Techniques* **2**, (1990) 16.
2. N. MUTO and H. YANAGIDA, *J. Am. Ceram. Soc.* **76** (1993) 1875.
3. K. K. CHAWLA, "Ceramic Matrix Composites" (Springer, New York, 1987).
4. A. G. EVANS and D. B. MARSHALL, *Acta Metall.* **37** (1989) 2567.
5. M. D. THOULESS, O. SBAIZERO, L. S. SIGL and A. G. EVANS, *J. Am. Ceram. Soc.* **72** (1989) 525.
6. E. BISCHOFF, M. RUHLE, O. SBAIZERO and A. G. EVANS, *ibid.* **72** (1989) 741.
7. K. M. PREWO, J. J. BRENNAN and G. K. LAYDEN, *Ceram. Bull.* **65** (1986) 305.
8. Dow Corning product data sheet, "Information About Nicalon Ceramic Fiber", Dow Corning Corporation, Midland, MI (1989).
9. R. F. COOPER and K. CHUNG, *J. Mater. Sci.* **22** (1987) 3148.
10. L. A. BONNEY and R. F. COOPER, *J. Am. Ceram. Soc.* **72** (1990) 2116.
11. P. M. BENSON, K. E. SPEAR and C. G. PANTANO, *Ceram. Eng. Sci. Proc.* **9** (1988) 663.
12. J. HOMENY, J. R. VAN VALZA and M. A. KELLY, *J. Am. Ceram. Soc.* **73** (1990) 2054.
13. H. H. SHIN, R. KIRCHAIN and R. F. SPEYER, *J. Mater. Res.* **10** (3) (1995) 602–608.
14. G. R. VILLALOBOS and R. F. SPEYER, "Proceedings of Symposium on Ceramic Matrix Composites", J. Am. Ceram. Soc. **74** Waterville, Ohio (1996).
15. D. B. MARSHALL, *J. Am. Ceram. Soc.* **47** (1984) C-259.



*Received 24 March*
*and accepted 29 May 1997*